Journal of Medicinal Chemistry

Article

Discovery of 1–(1H–Pyrazolo[4,3–c]pyridin–6–yl)urea Inhibitors of Extracellular Signal–Regulated Kinase (ERK) for the Treatment of Cancers

Jongwon Lim, Elizabeth H. Kelley, Joey L Methot, Hua Zhou, Alessia Petrocchi, Hongmin Chen, Susan E. Hill, Marlene C. Hinton, Alan Hruza, Joon O. Jung, John K. F. Maclean, My Mansueto, George N. Naumov, Ulrike Philippar, Shruti Raut, Peter Spacciapoli, Dongyu Sun, and Phieng Siliphaivanh

J. Med. Chem., **Just Accepted Manuscript** • DOI: 10.1021/acs.jmedchem.6b00708 • Publication Date (Web): 22 Jun 2016

Just Accepted

ACS Publications

Journal of Medicinal Chemistry is published by the American Chemical Society. 1155 Sixteenth Street N.W., Washington, DC 20036

Discovery of 1–(1*H*–Pyrazolo[4,3–*c*]pyridin–6–yl)urea Inhibitors of Extracellular Signal–Regulated Kinase (ERK) for the Treatment of Cancers

Jongwon Lim,*[,†] Elizabeth H. Kelley,[†] Joey L. Methot,[†] Hua Zhou,[†] Alessia Petrocchi,[†] Hongmin Chen,[‖] Susan E. Hill,[⊥] Marlene C. Hinton,[#] Alan Hruza,[∞] Joon O. Jung,[§] John K. F. Maclean,[§] My Mansueto,[‖] George N. Naumov,[#] Ulrike Philippar,[‡] Shruti Raut,[‖] Peter Spacciapoli,[‖] Dongyu Sun[‖] and Phieng Siliphaivanh[†]

Departments of [†]Chemistry, [‡]Oncology, [‖]In Vitro Pharmacology, [#]In Vivo Pharmacology, [§]Chemistry Modeling and Informatics, [⊥]Pharmacokinetics, Pharmacodynamics and Drug Metabolism, and [∞]Structural Chemistry, Merck & Co., Inc., 33 Avenue Louis Pasteur, Boston, MA 02115

Abstract

The ERK/MAPK pathway plays a central role in the regulation of critical cellular processes and is activated in more than 30% of human cancers. Specific BRAF and MEK inhibitors have shown clinical efficacy in patients for the treatment of BRAF–mutant melanoma. However, the majority of responses are transient, and resistance is often associated with pathway reactivation of the ERK signal pathway. Acquired resistance to these agents has led to greater interest in ERK, a downstream target of the MAPK pathway. De novo design efforts of a novel scaffold derived from SCH772984 by employing hydrogen bond interactions specific for ERK in the binding pocket identified 1–(1*H*–pyrazolo[4,3–*c*]pyridin–6–yl)ureas as a viable lead series. Sequential SAR studies led to the

identification of highly potent and selective ERK inhibitors with low molecular weight and high LE. Compound **21** exhibited potent target engagement and strong tumor regression in the $BRAF^{V600E}$ xenograft model.

KEYWORDS: ERK, MAPK, kinase inhibitors, 1–(1*H*–pyrazolo[4,3–*c*]pyridin–6–yl)urea, sequence conservation.

Introduction

The extracellular signal–regulated kinase (ERK) mitogen–activated protein kinase (MAPK) pathway plays a central role in the regulation of critical cellular processes such as cell proliferation, migration, and differentiation.[1] Activation of RAS leads to the recruitment and activation of RAF, a serine–threonine kinase. Activated RAF phosphorylates and activates MEK1/2, which then phosphorylates and activates ERK1/2. When activated, ERK1/2 phosphorylates several downstream targets involved in a multitude of cellular events including cytoskeletal changes and transcriptional activation. The ERK/MAPK pathway is activated in more than 30% of human cancers, most frequently via RAS and BRAF mutations, and thus has attracted significant interest as a therapeutic target for cancer.[2] Specific inhibitors of BRAF and its downstream effectors have been developed to target BRAF– and RAS–mutant tumors. In particular, the BRAF inhibitors, vemurafenib and dabrafenib, and the MEK inhibitor, trametinib, have been approved for the treatment of BRAF–mutant melanoma, and have shown clinical efficacy in patients.[3–5] However, the majority of responses are transient, and resistance is often associated with pathway reactivation of the ERK signal pathway.[6–8] The combination of the BRAF inhibitor dabrafenib with the MEK inhibitor trametinib has shown significant clinical benefit in BRAF–mutant melanoma compared with BRAF or MEK inhibitor monotherapy. However, drug–resistant tumor cells invariably emerged leading to disease progression. Acquired resistance to these agents has led to greater interest in ERK, a downstream target of the MAPK pathway.[9]

In 2013, researchers at Merck reported discovery and characterization of SCH772984 (**1**), a novel and selective inhibitor of ERK1/2 (Table 1).[10] Compound **1** has subnanomolar ERK2 potency and

nanomolar cellular potency in tumor cells with mutations in BRAF or RAS. Compound **1** inhibits not only the kinase activity of ERK (inhibition of pRSK) but also the phosphorylation of ERK by MEK (inhibition of pERK) via a large shift of the glycine rich loop of ERK upon binding.[11,12] This unique binding mode is believed to account for its excellent kinome selectivity (> 50% inhibition at 1 μM by 7 out of 309 kinases). Compound **1** induced tumor regressions in the xenograft models at tolerated doses. More importantly, **1** effectively inhibited MAPK signaling and cell proliferation in BRAF or MEK inhibitor–resistant models as well as in tumor cells resistant to concurrent treatment with BRAF and MEK inhibitors. These data support that pursuing ERK inhibition is a viable option for the treatment of tumors refractory to BRAF and MEK inhibitors.[13,14] In fact, the discovery of novel ERK inhibitors has been actively pursued by many research groups, and various classes of ERK inhibitors have been reported.[15–26]

Although **1** presented high ERK potency, excellent kinome selectivity, and high in vivo efficacy, its high molecular weight (MW 588) is suboptimal and may become a limitation. We pursued novel scaffolds that exhibit improved drug–like properties such as low molecular weight and high ligand efficiency (LE).[27] Herein, we report de novo design of a novel scaffold derived from **1** and a series of modifications to the scaffold. The SAR efforts led to the discovery of 1–(1*H*–pyrazolo[4,3–*c*]pyridin–6–yl)ureas as highly potent and selective ERK inhibitors with low molecular weight and high LE. In vivo efficacy results of compound **21** in a $BRAF^{V600E}$ xenograft model are also described.

Table 1. **Structure and Key Profile of SCH772984 (1)**

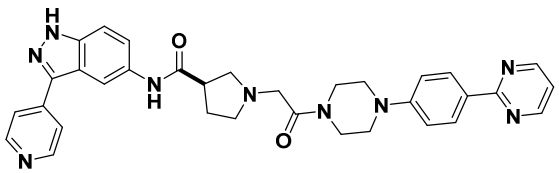

SCH772984 (1)

MW	588

hERK2 IC_{50} (nM)	0.4
LE	0.29
pRSK IC_{50} (nM)	57
pERK (A375) IC_{50} (nM)	9
A375SM Prolif IC_{50} (nM)	39
No. of Kinases Tested	309
Kinase Selectivity	7 kinases > 50% inhib @ 1 μM
FaSSIF Solubility (pH 6.5, μM)[a]	38

[a]FaSSIF = human fasted–state simulated intestinal fluid.

Chemistry

Scheme 1. Synthesis of the 1–(1*H*–Pyrazolo[4,3–*c*]pyridin–6–yl)ureas[a]

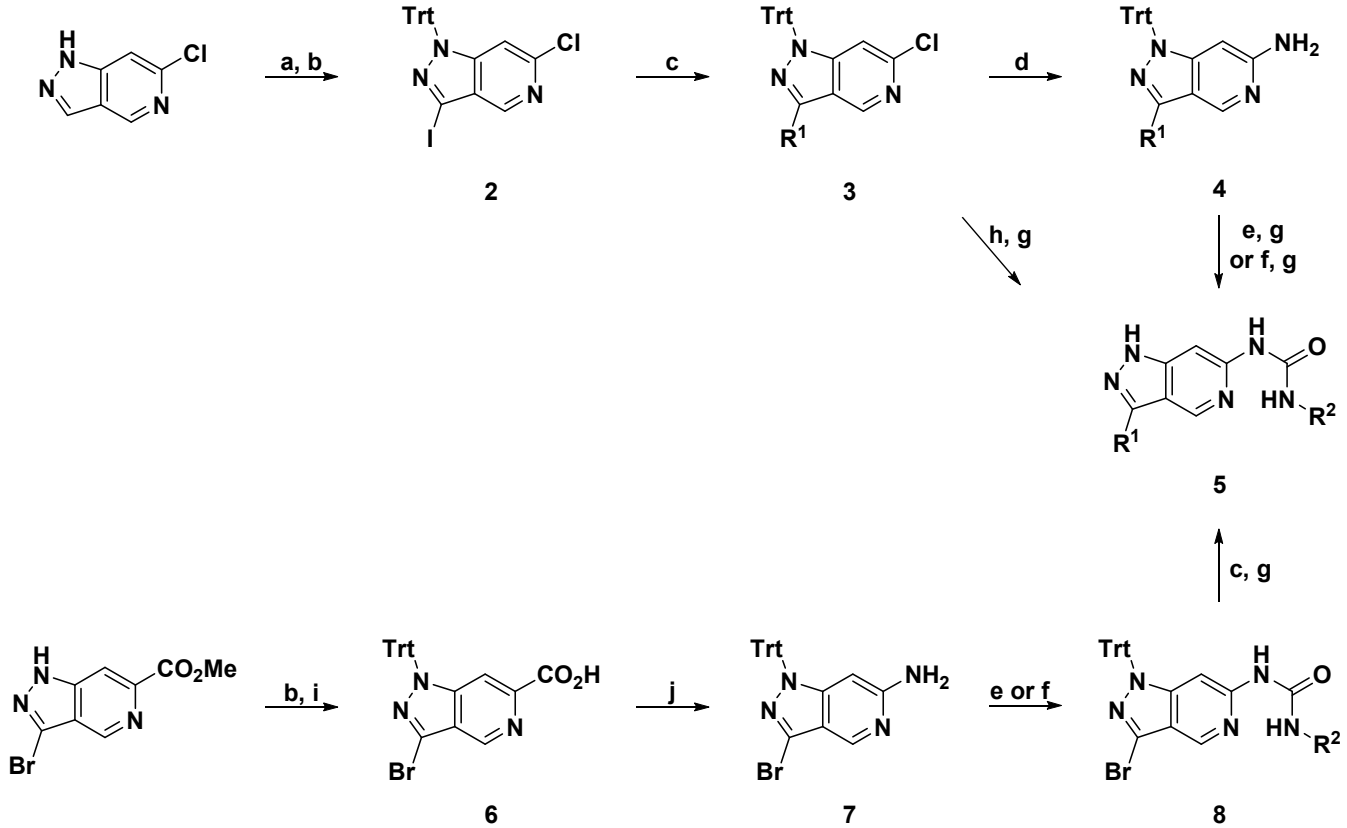

[a](a) I_2, KOH, DMF; (b) TrtCl, NaH, THF; (c) R^1–boronic acid or R^1–boronic ester, $PdCl_2(dppf)$, K_2CO_3, 1,4–dioxane/water, 80 °C; (d) LiHMDS, $Pd_2(dba)_3$, 2–(dicyclohexylphosphino)biphenyl, THF, 65 °C; (e) CDI, imidazole, DCM; R^2NH_2; (f) R^2NCO, 1,4–dioxane, 60 °C; (g) TFA, triethylsilane, DCM; (h) $R^2NHCONH_2$, BrettPhos precatalyst, Cs_2CO_3, DMA, 100 °C; (i) 1 N KOH, MeOH, 50 °C; (j) DPPA, TEA, 1,4–dioxane, 80 °C; 1 N KOH.

Synthetic routes for the 1–(1*H*–pyrazolo[4,3–*c*]pyridin–6–yl)ureas (**5**) are outlined in Scheme 1. Intermediate **2** was prepared starting from 6–chloro–1*H*–pyrazolo[4,3–*c*]pyridine via iodination at the C–3 position followed by protection of the 1*H*–pyrazole with a trityl group. Various substituents were

introduced to the C–3 position by employing Suzuki reaction[28] to afford **3**. The C6–Cl was then converted to the amino group via palladium mediated coupling conditions.[29] The amino group of intermediates **4** was reacted with either an array of amines in the presence of CDI or various isocyanates at an elevated temperature followed by sequential trityl group deprotection with TFA to afford ureas **5**. Alternatively, intermediates **3** were directly converted to **5** by employing palladium mediated coupling conditions with alkylureas followed by deprotection.[30] For a rapid derivatization at the C–3 position, intermediate **7** was converted to ureas **8** before various substituents were introduced to the C–3 position. Intermediate **7** was prepared via sequential protection with a trityl group, saponification, and Curtius rearrangement starting from methyl 3–bromo–1*H*–pyrazolo[4,3–*c*]pyridine–6–carboxylate.

Results and Discussions

Sequence Conservation in the ERK2 Binding Pocket.

Protein kinases regulate cellular signaling pathways by catalyzing phosphorylation of serine, threonine, and tyrosine residues of proteins in eukaryotic cells. Thus, protein kinases have emerged as promising therapeutic targets for many human diseases.[31] Small molecule protein kinase inhibitors have been widely used to elucidate the cellular and organismal roles of protein kinases. However, the ATP binding active site of human protein kinase domains is highly conserved even among distal human kinome families. Therefore, designing selective ATP–competitive inhibitors of a target kinase continues to be a daunting challenge.

Understanding the structural biology of the active site of a protein kinase is crucial for designing highly specific inhibitors for the kinase. To this end, we examined the sequence alignment of the ATP binding pocket of ERK compared to those of other kinases. We envisioned that we could improve kinase selectivity for ERK by implementing either favorable interactions between an inhibitor and residues distinct to ERK or unfavorable interactions between an inhibitor and residues common to off–target kinases. In the ATP binding pocket, there are several residues found in ERK with low frequency of

occurrence versus the kinome including Gln103 (1%), Lys112 (6%), Asp109 (7%), Tyr62 (10%), and Ser151 (11%) (Figure 1A). Especially, a combination of the gatekeeper Gln103 and Lys112 is only found in ERK1/2 out of 491 human kinases,[31] which presents an excellent opportunity for designing ERK selective inhibitors.

We pursued novel scaffolds derived from **1** that exhibit improved drug–like properties such as low molecular weight and high ligand efficiency.[27] First, we replaced the long side chain at the 5–position of the indazole, which takes up two–thirds of the molecular weight, with an amide group (**9** in Figure 1B). When **9** (R = Me) was docked to the ERK crystal structure, it was predicted to bind to the hinge and Lys112 in the same mode as **1** binds to the pocket (**9** in cyan in Figure 1C). However, **9** lacks the key interactions that the side chain of **1** makes, especially the π–π interaction between the terminal pyrimidine group of **1** and Tyr62 with concomitant shift of the glycine rich loop. The unique shift of the glycine rich loop and the π–π interaction with Tyr62 are believed to account for excellent kinome selectivity of **1**. Not surprisingly, **9** suffered significant erosion in kinase selectivity compared to **1** in a broad panel of kinome (data not shown).

We envisioned that we could overcome the loss in kinase selectivity by designing novel short side chains that are capable of making additional interactions with ERK residues that are not employed by **1**. Gln as a gatekeeper is very rare, occurring in only 1% of human kinases (*vide supra*), thus making a favorable interaction with Gln103 could significantly improve kinase selectivity for ERK. While **1** lacks a direct hydrogen bond interaction with Gln103,[11] other ERK inhibitors are known to employ a direct hydrogen binding to Gln103 in the literature.[15,16,18] Docking of **9** to the ERK crystal structure suggests that a hydrogen bond donor substituted at the 6–position, instead of the 5–position, would be pointing toward Gln103 within a hydrogen bond distance. To explore the gatekeeper interaction, we designed the 5–azaindole core with a urea group installed at the 6–position (**10** in Figure 1B). Compound **10** (R = Me) docks to the binding pocket in the same mode as **9** does (**10** in yellow in Figure 1C) making hydrogen bond interactions with the hinge and Lys112. Furthermore, the urea of **10** is positioned to make two

additional interactions with the enzyme, one with gatekeeper Gln103 and the other with catalytic Lys52. In this de novo design, the intramolecular hydrogen bonding between the 5–aza nitrogen and the urea nitrogen γ to the core is important as it would fix the urea bond α to the core to *s–trans* and direct the urea carbonyl group toward Lys52.

A)

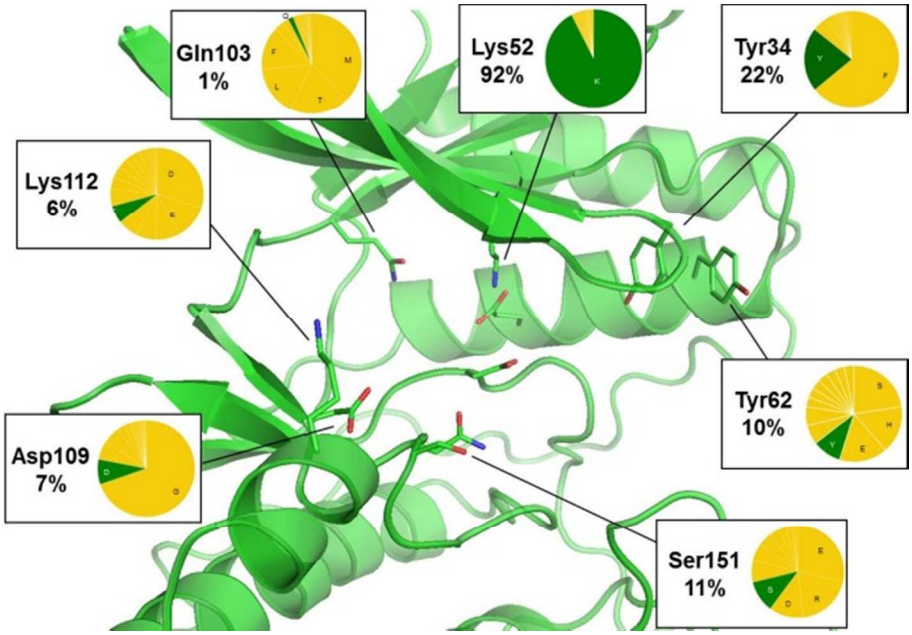

B)

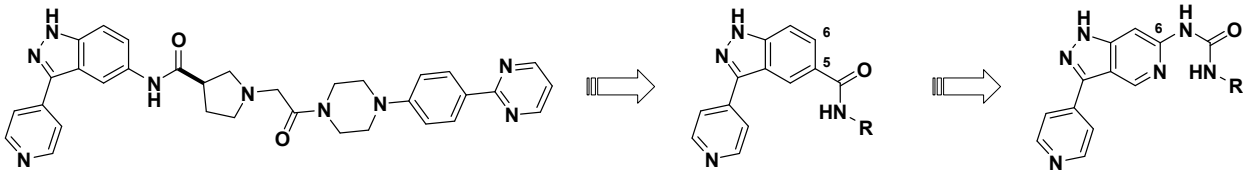

1 9 10

C)

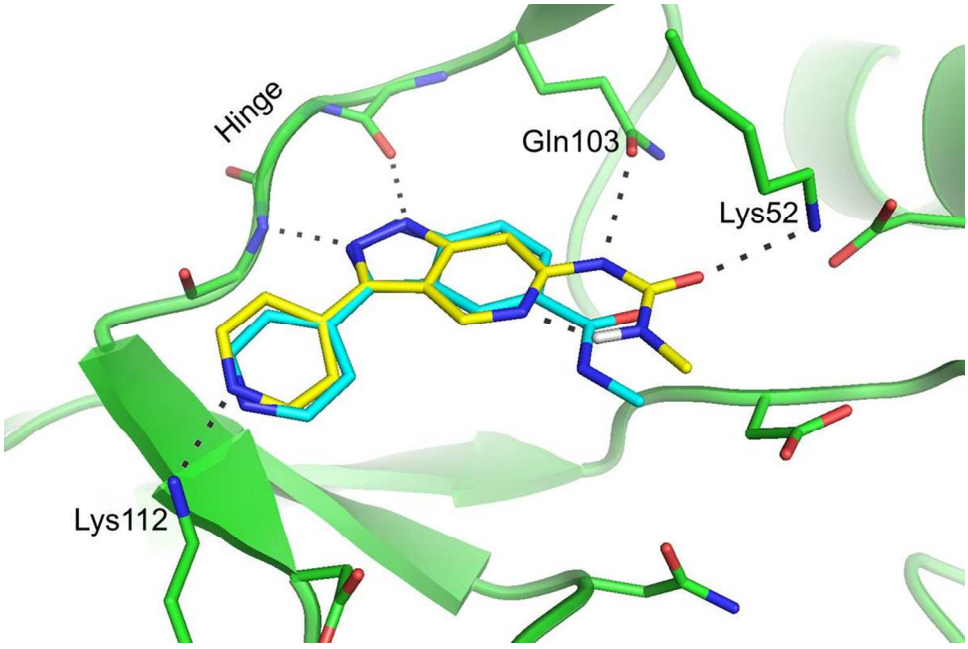

Figure 1. (A) Sequence conservation in the ERK2 binding pocket, (B) de novo design of the 1–(1*H*–pyrazolo[4,3–*c*]pyridin–6–yl)ureas, (C) docking of **9** (cyan) and **10** (yellow) to the binding pocket of ERK2.

Initial Exploration at C–6 of the 5–Azaindazole.

To test the hypothesis, we introduced a urea and other hydrogen bond donating groups at the 6–position of the 5–azaindazole. It was found that 2–methyl group on the pyridine at the 3–position afforded ameliorated CYP inhibitory profile of the molecules compared to the unsubstituted pyridine (data not shown), thus 2–methylpyridin–4–yl group was employed for our initial SAR studies (Table 2). Gratifyingly, the benzylurea analogue **11** was as potent as **1** in the ERK2 enzymatic assay, hinting that **11** might be making the envisioned hydrogen bond interactions with Gln103 and Lys52. The benzenepropanamide and the benzyl carbamate analogues (**12** and **13**), lacking the intramolecular hydrogen bond and favoring *s–cis* conformation of the amide and carbamate α to the core, were less potent than **11** by greater than 3 and 4 log units, respectively. The benzyl carbamate on the indazole core (**14**) was not tolerated at this position, either. The potency loss of these analogues confirmed the importance of the intramolecular hydrogen bond for efficient binding to ERK. The thiourea and the sulfamide analogues (**15** and **16**) suffered from loss of potency, albeit both would have the intramolecular hydrogen bond. Aminothiazoles at the 6–position were also pursued (**17** and **18**), where

the sulfur atom would have a favorable electrostatic interaction with the 5−aza nitrogen and the nitrogen of the thiazole ring would be positioned toward Lys52. However, compounds **17** and **18** displayed either greater than 60−fold loss of potency or a complete loss of potency, respectively.

Table 2. Initial SAR at C−6 of the Azaindazole

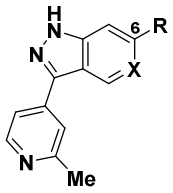

	X	R	hERK2 IC_{50} (nM)[a]	mERK2 IC_{50} (nM)[b]
11	N	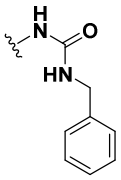	0.9	0.2
12	N	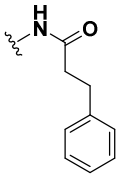	ND[c]	420
13	N	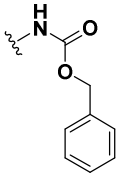	ND[c]	> 3,000
14	CH	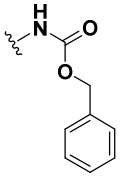	ND[c]	> 3,000
15	N	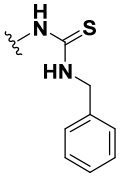	12	ND[c]

16	N	2,400	ND[c]
17	N	56	ND[c]
18	N	> 3,000	ND[c]

[a]human ERK2 IC_{50}. [b]mouse ERK2 IC_{50}. [c]ND = not determined.

Crystal Structure of Compound 11.

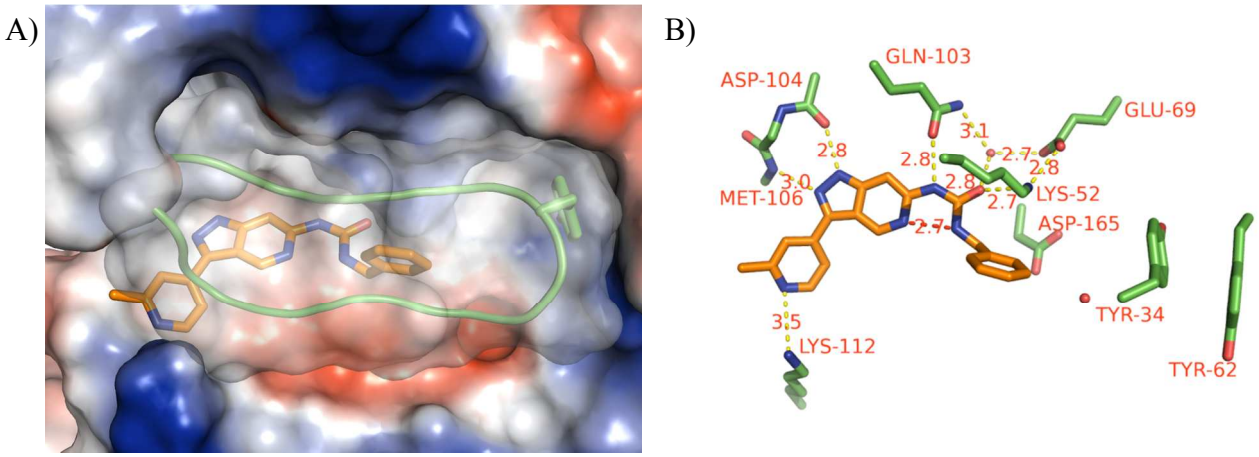

Figure 2. X–ray crystal structure of **11** bound to rat ERK2: (A) electrostatic surface view of the ERK2 active site bound to **11**. (B) hydrogen–bonding pattern in the structure of **11** bound to ERK2. Hydrogen bond distances are in Å.

The X–ray crystal structure of **11** bound to rat ERK2 confirmed the modeling hypothesis for the urea substitution interactions with the gatekeeper Gln103 (Figure 2). The 5–azaindazole moiety of **11** hydrogen bonds to the backbone carbonyl and amide nitrogen of hinge residues Asp104 and Met106, mimicking the indazole of **1**.[11] Lys112 sidechain forms a hydrogen bond to the nitrogen of methylpyridine as seen in **1**. The urea group forms an extensive hydrogen bonding network to the gatekeeper Gln103 sidechain, the side chain of the catalytic Lys52, and the sidechain of Glu69.

Compounds **11** and **1** have a conserved water, which is located in the back by the gatekeeper involved in the extensive hydrogen bonding network. Additionally, the urea nitrogen γ to the core makes an intramolecular hydrogen bond with the 5−aza nitrogen of the core, producing a nearly planar extension from the 5−azaindazole core. The benzyl group extends toward the glycine rich loop and does not disrupt the π−π stacking between Tyr34 and Tyr62 as found in the apo−form of ERK2, nor is there any major rearrangements of the C−helix or the DFG motif, unlike in the crystal structure of **1**.[11]

Exploration of the Urea Substituents.

Encouraged by high ERK potency of the novel 5−azaindazole with a urea group at the 6−position and novel hydrogen bond interactions confirmed by X−ray crystallography, we next focused on substituents on the urea. Throughout the SAR studies, key compounds were screened against a broad panel of kinases (101 or 265 kinases) to assess their kinome selectivity. When compound **11** was screened against a panel of 101 kinases, it showed greater than 100−fold selectivity against 95% of the kinases (Table 3). In the kinase counter−screening assays, coupled assays were employed for MEK1, RAF1, COT, and BRAF, where activity of the downstream kinase ERK was measured. Kinase selectivity of **11** is excellent considering that MEK1, RAF1, COT, and BRAF are 4 out of 5 off−targets inhibited by**11** with less than 100−fold selectivity.

While phenylurea **19** suffered from greater than 100−fold loss of the enzymatic potency, phenethylurea **20** displayed high potency comparable to **11** both in the enzymatic assay and in the cell biochemical assay, inhibition of phosphorylation of RSK (pRSK), downstream of ERK. Compound **20**, however, showed significant erosion in kinome selectivity (> 100−fold selective against 87% of the kinases). Major improvements in ERK potency were observed with methyl substituent at the benzylic position of the urea. Compared to **11**, (1*R*)−1−phenylethylurea **21** not only offered 3−fold improvement in cell potency (pRSK IC_{50} = 70 nM) but also maintained excellent kinase selectivity (> 100−fold selective against 97% of kinases in the panel of 265 kinases). It was found that stereochemistry at the benzylic

position was important, as the (*S*)−enantiomer **22** was greater than 20−fold less potent than **21**. The indane analogue **23**, tethering the benzylic methyl group to the benzene, showed greater than 5−fold loss of potency even if the more potent enantiomer of **23** was assumed to exclusively contribute to the potency.

Table 3. **SAR of the Urea Substituents**

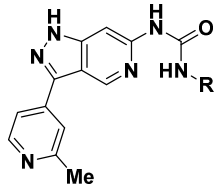

	R	hERK2 IC_{50} (nM)	pRSK IC_{50} (nM)[a]	No. of Kinases Tested	% of Kinases > 100×[b]
11	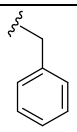	0.9	220	101	95
19		130	> 10,000	–	ND[c]
20	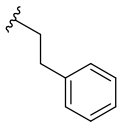	0.5[d]	110[e]	101	87
21	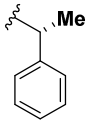	0.2	70	265	97
22	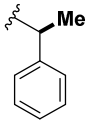	38[d]	1,800[e]	–	ND[c]
23	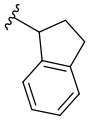	5	750	–	ND[c]

[a]From A375SM cells. [b]Fold selectivity against invitrogen ERK2 IC_{50}. [c]ND = not determined. [d]From mERK2 IC_{50} (nM). [e]From A375 cells.

Exploration of the C–3 Substituents.

Having identified promising (1*R*)–1–phenylethylurea substituent at the 6–position of the 5–azaindazole, we next explored various substituents at the 3–position of the 5–azaindazole core. Compared to **21**, the analogues with alkyl substituents such as n–propyl, cyclopropyl, and cyclopentyl groups at the 3–position (**24**, **25**, and **26**, respectively) suffered from loss of the cell potency by 5–11 fold (Table 4). Loss of the cell potency with the alkyl substituents, presumably due to absence of the interaction with Lys112, directed us toward exploring aromatic groups that could employ hydrogen bond interaction with Lys112. The 4–fluorophenyl, 2–methoxypyridin–4–yl, and 6–methylpyridazin–4–yl analogues (**28**, **31**, and **32**, respectively) also showed a loss of potency in the cell assay. On the other hand, the 1–methyl–1*H*–pyrazol–4–yl, 2,6–dimethylpyridin–4–yl, and 2–fluoropydin–4yl analogues (**27**, **29**, and **30**, respectively) offered comparable enzymatic and cell potency to **21**. While **27** displayed slight erosion in kinase selectivity, both **29** and **30** showed excellent selectivity in the broad panel of kinases.

While our SAR studies were primarily driven by on–target potency and kinome selectivity, activities against other off–targets such as hERG[32] and CYPs were closely monitored in parallel. Compounds **21**, **27**, **29**, and **30** offered satisfactory hERG activity profile (all IC_{50} > 20,000 nM) in addition to their excellent ERK potency and kinase selectivity. Compounds **27** and **29**, however, showed submicromolar activities in CYP3A4 inhibition (IC_{50} = 380 nM and 780 nM, respectively) while **21** and **30** offered more favorable CYP3A4 inhibitory activities (IC_{50} = 3,900 nM and 29,000 nM, respectively).

Table 4. **SAR of Substituents at the C–3 Position**

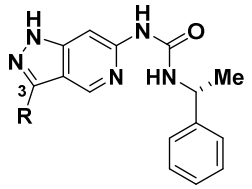

R	hERK2 IC_{50} (nM)	pRSK IC_{50} (nM)[a]	No. of Kinases Tested	% of Kinases > 100×[b]

21	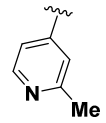	0.2	70	265	97
24		2	350	101	96
25		2	550	101	95
26		4	810	–	ND[c]
27	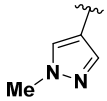	0.3	110	101	94
28	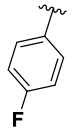	0.8	360	101	96
29	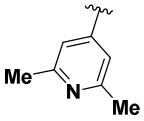	0.3	130	101	99
30	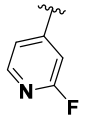	0.3	97	101	96
31	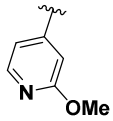	0.9	300	–	ND[c]
32	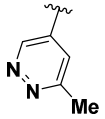	0.9	810	–	ND[c]

[a]From A375SM cells. [b]Fold selectivity against invitrogen ERK2 IC_{50}. [c]ND = not determined.

Cell Activity and PK Profile of 21.

Compared to **1**, compound **21** inhibits ERK with the same potency level in pRSK and A375SM ($BRAF^{V600E}$) proliferation assays (IC_{50} = 43 nM) with a fraction of molecular weight (MW 372 *vs* 588), thereby offers much higher ligand efficiency[27] (LE 0.46 *vs* 0.29) (Table 5). One stark difference between **1** and **21** is that **1** inhibits phosphorylation and activation of ERK (pERK IC_{50} = 9 nM) while

21 does not (pERK IC_{50} > 10,000 nM). Compound **21** showed excellent kinome selectivity comparable to **1**, hitting only 8 kinases with less than 100−fold selectivity out of 265 kinases tested. Compound **21** was weakly active in the wild−type CHL−1 proliferation assay (IC_{50} = 1,300 nM), confirming its high selectivity for ERK/MAPK pathway. Compound **21** displayed PK properties in rats (Cl_p = 35 mL/min/kg, F = 12%) suitable for in vivo studies. While its polarity is within a good range judged by cLogD value, its modest solubility is suboptimal.

Table 5. Profile of 21

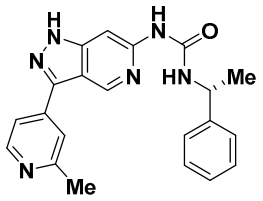

20

MW	372
hERK2 IC_{50} (nM)	0.2
LE	0.46
pRSK IC_{50} (nM)	77
pERK IC_{50} (nM)	> 10,000
A375SM Prolif IC_{50} (nM)	43
CHL−1 Prolif IC_{50} (nM)	1,300
No. of Kinases Tested	265
Kinases < 100×[a]	BRAF, ERK1, FLT4, MEK1, MEK2, MELK, $PDGFRA^{D842V}$, $PDGFRA^{V561D}$
Rat PK Properties	
AUC_{norm} (μM·h/mpk)[b]	1.3
Cl_p (mL/min/kg)[b]	35
V_{dss} (L/kg)[b]	1.7
$t_{1/2}$ (h)[b]	0.7
Bioavailability (%)[c]	12
Physical Properties	
cLogD (pH 7.4)[d]	2.2

Rat plasma protein binding (%)	98.8
FaSSIF Solubility (pH 6.5, μM)[e]	18

[a]Fold selectivity against invitrogen ERK2 IC_{50}. [b]Dosed IV at 0.5 mg/kg as a solution in PEG400:H_2O (60:40 (v/v)). [c]Dosed PO at 1 mg/kg as a solution in PEG400:H_2O (60:40 (v/v)). [d]At pH 7.4 from ACD Labs v10. [e]FaSSIF = human fasted–state simulated intestinal fluid.

In Vivo Studies of 21.

On the basis of its excellent ERK cell potency both in pRSK and proliferation assays, clean off–target kinase activity profile, and PK properties suitable for oral dosing in rats, compound **21** was chosen for in vivo proof–of–mechanism studies. In this in vivo xenograft model, mice bearing A375SM tumor xenograft were dosed with either vehicle or compound **21** orally at 25 mg/kg BID, 50 mg/kg BID, and 100 mg/kg QD for 20 days. After the final dose on day 20, blood samples from the vehicle arm and the 100 mg/kg QD arm were obtained at various time points, and exposure of **21** and pRSK as well as pERK levels were measured (Figure 3A). The mice dosed with **21** exhibited potent and sustained inhibition of pRSK in response to the exposure level of **21**, while durable inhibition of pERK was not observed. These results confirm the inhibitory activity of ERK by **21** in vivo. Compared to the mice treated with vehicle, the mice treated with **21** showed either tumor growth inhibition (82% at 25 mg/kg BID) or tumor regression (47% at 50 mg/kg BID; 42% at 100 mg/kg QD) in a dose dependent manner (Figure 3B). The plasma exposure of **21** on day 20 displayed a strong correlation between the exposure and the efficacy (Table 6). The strong efficacy of **21** in this mouse model supports that inhibition of ERK activity without inhibition of ERK activation, as judged by sustained inhibition of pRSK and lack of durable inhibition of pERK (Figure 3A), could be a viable option for the treatment of cancers.

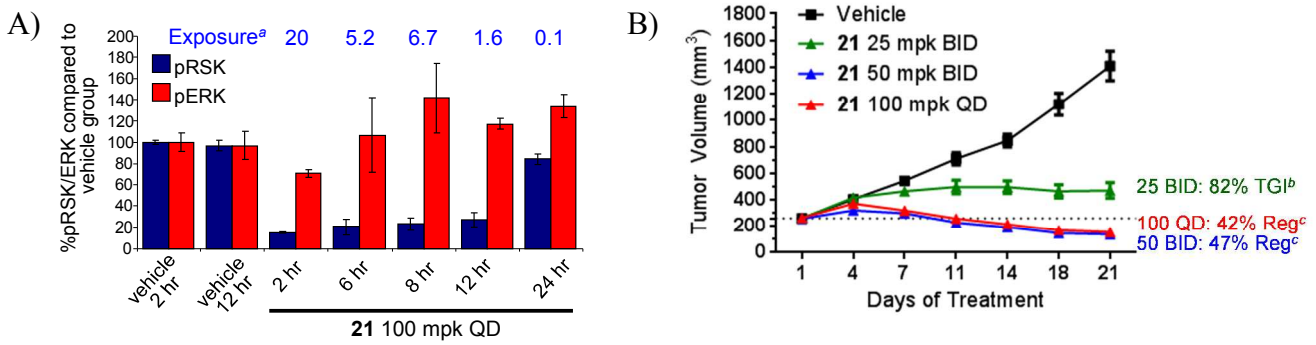

Figure 3. Effect of **21** in A375SM xenograft model. Compound **21** was dosed orally as a solution in PEG300:H_2O (50:50 (v/v)). (A) PK/PD of the 100 mpk QD arm of **21** compared to the vehicle treated arm on day 20. [a]Exposure of **21** in μM from the 100 mg/kg QD arm after the final dose on day 20. (B) Effect of **21** in tumor volume compared to the vehicle treated arm. [b]tumor growth inhibition. [c]tumor regression.

Table 6. Exposure of 21 on day 20 in A375SM xenograft model.

Dosing Regimen of **21**[a]	AUC (μM·h)[b]	C_{max} (μM)[c]	T_{max} (h)[d]
25 mpk BID	95	12	11
50 mpk BID	240	23	11
100 mpk QD	320	27	4

[a]Compound **21** was dosed orally as a solution in PEG300:H_2O (50:50 (v/v)). [b]Area under the curve. [c]Peak plasma concentration. [d]Time to reach C_{max}.

Conclusions

A novel 1–(1*H*–pyrazolo[4,3–*c*]pyridin–6–yl)urea scaffold was successfully designed by installing a urea group at the 6–position of the 5–azaindazole core. In addition to the hydrogen bonds with the hinge and Lys52, the scaffold employs hydrogen bond interactions with gatekeeper Gln103 and Lys112, which are unique to ERK out of 491 human kinases. The interactions with the residues specific to ERK in otherwise highly conserved binding pocket of kinases account for excellent kinome selectivity of 1–(1*H*–pyrazolo[4,3–*c*]pyridin–6–yl)ureas. SAR studies on the 6–position of the 5–azaindazole core led to identification of (1*R*)–1–phenylethylurea as an optimal substituent. Subsequent exploration of the C–3 substituents identified both 2–methylpyridin–4–yl and 2–fluoropyridin–4–yl groups that offered

high ERK potency as well as low off−target activities. Compound **21** is highly potent in the target engagement and the proliferation assays in a pathway specific manner, and highly selective for ERK in the kinome panel. In the $BRAF^{V600E}$ xenograft model, **21** exhibited potent target engagement and strong tumor regression in a dose dependent manner, demonstrating a potential of ERK inhibitors as an anti−cancer agent.

Experimental

Chemistry. Commercial reagents were obtained from reputable suppliers and used as received. All solvents were purchased in septum−sealed bottles stored under an inert atmosphere. All reactions were sealed with septa through which an argon atmosphere was introduced unless otherwise noted. Liquid reagents and solvents were transferred under a positive pressure of nitrogen via syringe. Reactions were conducted in microwave vials or round bottomed flasks containing Teflon−coated magnetic stir bars. Microwave reactions were performed with a Biotage Initiator Series Microwave (fixed hold time setting; reaction temperatures monitored by the internal infrared sensor).

Reactions were monitored by thin layer chromatography (TLC) on pre−coated TLC glass plates (silica gel 60 F254, 250 μm thickness) or by LC/MS (30 mm x 2 mm 2 μm column + guard; 2 μL injection; 3% to 98% MeCN/water + 0.05% TFA gradient over 2.3 minutes; 0.9 mL/min flow; ESI; positive ion mode; UV detection at 254 nm). Visualization of the developed TLC chromatogram was performed by fluorescence quenching. Flash chromatography was performed on an automated purification system using pre−packed silica gel columns. ^{1}H NMR spectra were recorded on either a 500 or a 600 MHz Varian spectrometer; chemical shifts (δ) are reported relative to residual proton solvent signals. Data for NMR spectra are reported as follows: chemical shift (δ ppm), multiplicity (s = singlet, brs = broad singlet, d = doublet, t = triplet, q = quartet, dd = doublet of doublets, td = triplet of doublets, m = multiplet), coupling constant (Hz), integration.

All tested compounds reported are of at least 95% purity, as judged by LCAP (150 mm x 4.6 mm ID, 5 μm column; 5 μL injection; 10–100% MeCN/H_2O + 0.05% TFA gradient over 6.75 min; 1 mL/min flow; ESI; positive ion mode; UV detection at 254 nm, Bw8).

6–Chloro–3–iodo–1–trityl–1*H*–pyrazolo[4,3–*c*]pyridine (**2**). *Step 1*. A flask was charged with 6–chloro–1*H*–pyrazolo[4,3–*c*]pyridine (3.0 g, 19.5 mmol), iodine (13.1 g, 51.7 mmol), KOH (3.29 g, 58.6 mmol), and DMF (60 mL). The mixture was heated to 40 °C for 16 h and then additional iodine (7.8 g, 30.7 mmol) and KOH (1.6 g, 28.4 mmol) were added. The mixture was heated to 70 °C for 3 h, treated with 1N $Na_2S_2O_3$ solution, and extracted with EtOAc (3×). The combined organics were washed with water and brine, dried over sodium sulfate, and concentrated. DCM was added to the residue and the solid was collected by filtration to afford 6–chloro–3–iodo–1*H*–pyrazolo[4,3–*c*]pyridine (3.2 g, 11.5 mmol, 59% yield) as a yellow solid. LRMS (ESI) calcd for ($C_6H_4ClIN_3$) $[M + H]^+$ 280, found 280. ^{1}H NMR (600 MHz, DMSO–d_6) δ 14.00 (s, 1H), 8.63 (s, 1H), 7.68 (s, 1H).

Step 2. To a stirred solution of 6–chloro–3–iodo–1*H*–pyrazolo[4,3–*c*]pyridine (1.87 g, 6.71 mmol) in THF (20 mL) was added NaH (60% in mineral oil, 0.40 g, 10.1 mmol) at 0 °C and the mixture was stirred for 50 min at 0 °C. Trityl chloride (2.24 g, 8.05 mmol) was added at the same temperature and the mixture was stirred at room temperature for 16 h, treated with saturated NH_4Cl solution, and extracted with EtOAc (3×). The combined organics were washed with water and brine, dried over sodium sulfate, concentrated, and purified by flash chromatography to afford **2** (3.26 g, 6.25 mmol, 93% yield) as a light yellow solid. LRMS (ESI) calcd for ($C_{25}H_{18}ClIN_3$) $[M + H]^+$ 522, found 522. ^{1}H NMR (600 MHz, $CDCl_3$) δ 8.54 (s, 1H), 7.14–7.33 (m, 15H), 6.01 (s, 1H).

6–Chloro–3–(2–methylpyridin–4–yl)–1–trityl–1*H*–pyrazolo[4,3–*c*]pyridine (**3**, R^1 = 2–methylpyridinyl). A mixture of **2** (2.47 g, 4.72 mmol), 2–methylpyridine–4–boronic acid (0.97 g, 7.05 mmol), $PdCl_2$(dppf)–CH_2Cl_2 adduct (0.58 g, 0.71 mmol), and K_2CO_3 (1.96 g, 14.2 mmol) in 1,4–dioxane (10 mL) and H_2O (2.5 mL) was purged with nitrogen for 5 min, heated to 80 °C overnight,

cooled to room temperature, and diluted with EtOAc. The reaction mixture was filtered through Celite and then partitioned between EtOAc and saturated $NaHCO_3$ solution. The organic layer was extracted with EtOAc (3×) and the combined organics were dried over sodium sulfate and concentrated. The residue was purified by flash chromatography to afford **3** (R^1 = 2–methylpyridinyl) (1.02 g, 2.09 mmol, 44% yield). LRMS (ESI) calcd for ($C_{31}H_{24}ClN_4$) $[M + H]^+$ 487, found 487. ^{1}H NMR (600 MHz, DMSO–d_6) δ 9.42 (s, 1H), 8.56 (d, J = 4.8 Hz, 1H), 7.81 (s, 1H), 7.69 (d, J = 5.4 Hz, 1H), 7.19–7.41 (m, 15H), 6.09 (s, 1H), 2.56 (s, 3H).

3–(2–Methylpyridin–4–yl)–1–trityl–1*H*–pyrazolo[4,3–*c*]pyridin–6–amine (**4**, R^1 = 2–methylpyridinyl). $Pd_2(dba)_3$ (0.19 g, 0.21 mmol), 2–(dicyclohexylphosphino)biphenyl (0.073 g, 0.21 mmol), and **3** (R^1 = 2–methylpyridinyl) (1.02 g, 2.09 mmol) were placed in a microwave vial under nitrogen and dissolved in THF (11 mL). The reaction mixture was purged with nitrogen for 5 min, treated with LiHMDS (1 M in THF, 2.51 mL, 2.51 mmol), and heated to 65 °C overnight. The mixture was cooled to room temperature and treated with additional amounts of $Pd_2(dba)_3$ (0.096 g, 0.1 mmol), 2–(dicyclohexylphosphino)biphenyl (0.036 g, 0.1 mmol) and LiHMDS (1 M in THF, 1.25 mL, 1.25 mmol). The mixture was purged with nitrogen for 5 min, heated to 80 °C for 3 h, cooled to room temperature, and treated with 1N HCl. The mixture was concentrated and partitioned between DCM and 1N NaOH. The organic layer was extracted with DCM (3×) and the combined organics were dried over sodium sulfate and concentrated. The residue was purified by flash chromatography to afford **4** (R^1 = 2–methylpyridinyl) (549 mg, 2.09 mmol, 56% yield) as a solid. LRMS (ESI) calcd for ($C_{31}H_{26}N_5$) $[M + H]^+$ 468, found 468. ^{1}H NMR (600 MHz, DMSO–d_6) δ 8.93 (d, J = 1.2 Hz, 1H), 8.49 (d, J = 4.8 Hz, 1H), 7.68 (s, 1H), 7.58 (dd, J = 5.4, 1.2 Hz, 1H), 7.20–7.38 (m, 15H), 5.84 (s, 2H), 5.38 (d, J = 1.2 Hz, 1H), 2.53 (s, 3H).

3–Bromo–1–trityl–1*H*–pyrazolo[4,3–*c*]pyridine–6–carboxylic acid (**6**). *Step 1*. To a brown suspension of methyl 3–bromo–1*H*–pyrazolo[4,3–*c*]pyridine–6–carboxylate (5.0 g, 19.5 mmol) in DMF (50 mL) was added NaH (60% in mineral oil, 1.17 g, 29.3 mmol) in portions at 0 °C. The reaction

mixture was stirred at that temperature for 30 min, and a solution of trityl chloride (6.53 g, 23.4 mmol) in DMF (50 mL) was added dropwise. The reaction mixture was slowly warmed to room temperature and left to stir overnight. The reaction mixture was treated with water and extracted with EtOAc (3×). The combined organics were washed with brine, dried over sodium sulfate, concentrated, and purified by flash chromatography to afford methyl 3–bromo–1–trityl–1*H*–pyrazolo[4,3–*c*]pyridine–6–carboxylate as a white solid (6.0 g, 12.0 mmol, 62% yield). LRMS (ESI) calcd for ($C_{27}H_{21}BrN_3O_2$) $[M + H]^+$ 498, found 498. ^{1}H NMR (600 MHz, $CDCl_3$) δ 8.99 (s, 1H), 7.16–7.34 (m, 15H), 6.92 (s, 1H), 3.89 (s, 3H).

Step 2. To a suspension of methyl 3–bromo–1–trityl–1*H*–pyrazolo[4,3–*c*]pyridine–6–carboxylate (6.0 g, 12.0 mmol) in MeOH (60 mL) was added 1N KOH (42.1 mL, 42.1 mmol). The reaction mixture was heated to 50 ^{o}C for 1 h. The mixture was cooled to room temperature and acidified to pH 4 with 1N HCl. The precipitate was filtered, washed with water, and dried to afford **6** (5.3 g, 11 mmol, 91% yield). LRMS (ESI) calcd for ($C_{26}H_{19}BrN_3O_2$) $[M + H]^+$ 484, found 484. ^{1}H NMR (600 MHz, DMSO–d_6) δ 13.16 (brs, 1H), 9.02 (s, 1H), 7.15–7.39 (m, 15H), 6.92 (s, 1H).

3–Bromo–1–trityl–1*H*–pyrazolo[4,3–*c*]pyridin–6–amine (**7**). To a suspension of **6** (1.95 g, 4.03 mmol) in 1,4–dioxane (20 mL) was added a solution of diphenylphosphoryl azide (DPPA) (1.047 mL, 4.83 mmol) and TEA (0.842 mL, 6.04 mmol) in 1,4–dioxane (10 mL) dropwise over 5 min. The clear solution was heated to 80 ^{o}C for 2 h and treated with 1N KOH (20.1 mL, 20.1 mmol) at that temperature. The reaction mixture was heated to 80 ^{o}C overnight, cooled to room temperature, and extracted with EtOAc (3×). The combined organics were washed with brine, dried over sodium sulfate, concentrated, and purified by flash chromatography to afford **7** (0.61 g, 1.3 mmol, 33% yield) as an off–white solid. LRMS (ESI) calcd for ($C_{25}H_{20}BrN_4$) $[M + H]^+$ 455, found 455. ^{1}H NMR (600 MHz, DMSO–d_6) δ 8.28 (s, 1H), 7.18–7.35 (m, 15H), 5.97 (s, 2H), 5.31 (s, 1H).

1–(3–bromo–1–trityl–1*H*–pyrazolo[4,3–*c*]pyridin–6–yl)–3–[(1*R*)–1–phenylethyl]urea (**8**, R^2 = (1*R*)–1–phenylethyl). To a flask were added **7** (500 mg, 1.10 mmol), CDI (356 mg, 2.20 mmol),

imidazole (150 mg, 2.20 mmol), and DCM (11 mL). The mixture was stirred at room temperature for 16 h, treated with (1*R*)–1–phenylethanamine (272 mg, 2.25 mmol), and left to stir for 1 h. The mixture was purified by flash chromatography to afford **8** (R^2 = (1*R*)–1–phenylethyl) (582 mg, 0.966 mmol, 88% yield) as a white solid. LRMS (ESI) calcd for ($C_{34}H_{29}BrN_5O$) $[M + H]^+$ 602, found 602. ^{1}H NMR (600 MHz, $CDCl_3$) δ 9.59 (s, 1H), 8.52 (s, 1H), 7.02–7.31 (m, 21H), 5.33 (s, 1H), 5.01 (m, 1H), 1.50 (d, *J* = 7.2 Hz, 3H).

(*R*)–1–(1–Phenylethyl)urea. A mixture of (*R*)–1–phenylethylamine (1.00 g, 8.25 mmol) in water (4 mL) was treated with HCl (1 N, 8.5 mL, 8.5 mmol) followed by potassium cyanate (3.35 g, 41.2 mmol). The reaction mixture was warmed to 80 °C for 1 hour and cooled to room temperature. The mixture was neutralized with saturated $NaHCO_3$ solution and extracted with EtOAc and 2–methyltetrahydrofuran. The combined organics were dried over sodium sulfate, concentrated, and purified by flash chromatography to afford (*R*)–1–(1–Phenylethyl)urea (1.32 g, 8.04 mmol, 97% yield) as a white solid. LRMS (ESI) calcd for $C_9H_{13}N_2O$) $[M + H]^+$ 165, found 165. ^{1}H NMR (600 MHz, DMSO–d_6) δ 7.23–7.28 (m, 4 H), 7.17 (t, *J* = 6.7 Hz, 1 H), 6.38 (d, *J* = 7.9 Hz, 1 H), 5.38 (br s, 2 H), 4.65 (m, 1 H), 1.26 (d, *J* = 7.1 Hz, 3 H).

1–Benzyl–3–[3–(2–methylpyridin–4–yl)–1*H*–pyrazolo[4,3–*c*]pyridin–6–yl]urea (**11**). *Step 1*. To a stirred solution of CDI (520 mg, 3.21 mmol) in DCM (3 mL) was added a solution of **3** (R^1 = 2–methylpyridinyl) (300 mg, 0.642 mmol) and imidazole (131 mg, 1.93 mmol) in DCM (3 mL). The mixture was left to stir overnight and treated with benzylamine (344 mg, 3.21 mmol). The reaction mixture was left to stir for 2 h and purified by flash chromatography to afford a solid, which was directly dissolved in DCM (20 mL) and treated with triethylsilane (75 mg, 0.64 mmol) and TFA (4 mL). The reaction mixture was left to stir overnight, concentrated, diluted with saturated sodium bicarbonate solution, and extracted with chloroform:*i*–PrOH (3:1, 3×). The combined organics were dried over sodium sulfate, concentrated, and purified by flash chromatography to afford **11** (167 mg, 0.47 mmol, 73% yield). HRMS (ESI) calcd for ($C_{20}H_{19}N_6O$) $[M + H]^+$ 359.1620, found 359.1623. ^{1}H NMR (600

MHz, DMSO–d_6) δ 13.5 (s, 1H), 9.28 (s, 1H), 9.23 (s, 1H), 8.55 (d, J = 5.4 Hz, 1H), 7.89 (s, 1H), 7.81 (d, J = 5.4 Hz, 1H), 7.71–7.79 (m, 2H), 7.25–7.37 (m, 5H), 4.39 (d, J = 6.0 Hz, 2H), 2.58 (s, 3H).

1–[3–(2–Methylpyridin–4–yl)–1*H*–pyrazolo[4,3–*c*]pyridin–6–yl]–3–[(1*R*)–1–phenylethyl]urea (**21**). Prepared in analogy to that described for **11** in 83% yield. HRMS (ESI) calcd for ($C_{21}H_{21}N_6O$) [M + H]$^+$ 373.1777, found 373.1779. ^{1}H NMR (600 MHz, DMSO–d_6) δ 13.49 (s, 1H), 9.24 (s, 1H), 9.13 (s, 1H), 8.55 (d, J = 4.8 Hz, 1H), 7.89 (s, 1H), 7.81 (d, J = 4.2 Hz, 1H), 7.35–7.56 (m, 2H), 7.24–7.39 (m, 5H), 4.90 (m, 1H), 2.58 (s, 3H), 1.43 (d, J = 7.2 Hz, 3H).

1–(2,3–Dihydro–1*H*–inden–1–yl)–3–[3–(2–methylpyridin–4–yl)–1*H*–pyrazolo[4,3–*c*]pyridin–6–yl]urea trifluoroacetate (**23**). Prepared in analogy to that described for **11** in 23% yield. HRMS (ESI) calcd for ($C_{22}H_{21}N_6O$) [M + H]$^+$ 385.1777, found 385.1787. ^{1}H NMR (600 MHz, DMSO–d_6) δ 14.00 (s, 1H), 9.37 (s, 1H), 9.23 (s, 1H), 8.77 (d, J = 6.6 Hz, 1H), 8.41 (s, 1H), 8.33 (brs, 1H), 7.94 (s, 1H), 7.55 (brs, 1H), 7.22–7.32 (m, 4H), 5.26 (m, 1H), 2.77 (s, 3H), 1.28–2.97 (m, 4H).

***N*–[3–(2–Methylpyridin–4–yl)–1*H*–pyrazolo[4,3–*c*]pyridin–6–yl]–3–phenylpropanamide** (**12**). To a stirred mixture of **3** (R^1 = 2–methylpyridinyl) (53.2 mg, 0.114 mmol), 3–phenylpropionic acid (27.3 mg, 0.182 mmol) and 2–chloro–1–methylpyridinium iodide (49 mg, 0.19 mmol) in DCE (1 mL) was added TEA (0.048 mL, 0.34 mmol). The reaction mixture was heated to 70 °C for 1 h, cooled to room temperature, diluted with EtOAc and saturated sodium bicarbonate solution, and extracted with EtOAc (3×). The combined organics were dried over sodium sulfate and concentrated. The residue was dissolved in DCM (1.5 mL), treated with triethylsilane (0.018 mL, 0.11 mmol) and TFA (0.15 mL), and left to stir overnight. The mixture was concentrated and purified by preparative–HPLC. The collected fractions were partitioned between EtOAc and saturated sodium bicarbonate solution and extracted with EtOAc (3×). The combined organics were dried over sodium sulfate and concentrated to afford **12** (17 mg, 0.048 mmol, 42% yield). HRMS (ESI) calcd for ($C_{21}H_{20}N_5O$) [M + H]$^+$ 358.1668, found 358.1670. ^{1}H NMR (600 MHz, DMSO–d_6) δ 13.66 (s, 1H), 10.72 (s, 1H), 9.30 (s, 1H), 8.57 (d, J = 5.4 Hz, 1H),

8.29 (s, 1H), 7.91 (s, 1H), 7.85 (d, *J* = 4.8 Hz, 1H), 7.18–7.30 (m, 5H), 2.93 (t, *J* = 7.8 Hz, 2H), 2.76 (t, *J* = 7.8 Hz, 2H), 2.59 (s, 3H).

1–Benzyl–3–[3–(2–methylpyridin–4–yl)–1*H*–pyrazolo[4,3–*c*]pyridin–6–yl]thiourea (**15**). A suspension of **3** (R^1 = 2–methylpyridinyl) (25 mg, 0.05 mmol) in toluene (1 mL) was treated with (isothiocyanatomethyl)benzene (15 mg, 0.1 mmol) and the mixture was heated to 100 °C overnight. The mixture was cooled to room temperature and concentrated. The residue was dissolved in DCM (0.8 mL), treated with TFA (0.2 mL) and triethylsilane (0.008 mL, 0.05 mmol), left to stir for 5 h, concentrated, and purified by preparative–HPLC to afford **15** trifluoroacetate (7 mg, 0.014 mmol, 27% yield) as a yellow solid. HRMS (ESI) calcd for ($C_{20}H_{19}N_6S$) $[M + H]^+$ 375.1392, found 375.1402. ^{1}H NMR (600 MHz, DMSO–d_6) δ 11.95 (br s, 1H), 10.77 (s, 1H), 9.35 (s, 1H), 8.69 (d, *J* = 5.0 Hz, 1H), 8.27 (s, 1H), 8.18 (br s, 1H), 7.55–7.24 (m, 5H), 7.14–7.10 (m, 1H), 4.92 (d, *J* = 5.3 Hz, 2H), 2.67 (s, 3H).

3–(2–Methylpyridin–4–yl)–*N*–(1,3–thiazol–2–yl)–1*H*–pyrazolo[4,3–*c*]pyridin–6–amine trifluoroacetate (**17**). A suspension of **3** (R^1 = 2–methylpyridinyl) (42 mg, 0.090 mmol) in 1,4–dioxane (0.5 mL) was treated with sodium hydride (60%, 18 mg, 0.45 mmol), left to stir for 10 min, and treated with 2–chlorothiazole (0.012 mL, 0.14 mmol). The mixture was heated to 90 °C for 3.5 h, cooled to room temperature, diluted with EtOAc, washed with saturated sodium bicarbonate solution, and concentrated. The residue was dissolved in DCM (0.8 mL), treated with of TFA (0.2 mL) and triethylsilane (0.014 mL, 0.090 mmol), and left to stir for 2 h. The mixture was concentrated and purified by preparative–HPLC to afford **17** trifluoroacetate (22 mg, 0.052 mmol, 58% yield) as a yellow solid. HRMS (ESI) calcd for ($C_{15}H_{13}N_6S$) $[M + H]^+$ 309.0922, found 309.0923. ^{1}H NMR (600 MHz, DMSO–d_6) δ 13.96 (s, 1H), 11.33 (brs, 1H), 9.54 (s, 1H), 8.79 (d, *J* = 6.6 Hz, 1H), 8.49 (s, 1H), 8.38 (brs, 1H), 7.40 (d, *J* = 3.6 Hz, 1H), 7.37 (s, 1H), 7.03 (d, *J* = 3.6 Hz, 1H), 2.80 (s, 3H).

3–(2–Methylpyridin–4–yl)–*N*–(5–phenyl–1,3–thiazol–2–yl)–1*H*–pyrazolo[4,3–*c*]pyridin–6–amine trifluoroacetate (**18**). Prepared in analogy to that described for **17** in 32% yield. HRMS (ESI) calcd for

($C_{21}H_{17}N_6S$) $[M + H]^+$ 385.1235, found 385.1242. ^{1}H NMR (600 MHz, DMSO–d_6) δ 14.05 (s, 1H), 11.47 (brs, 1H), 9.62 (s, 1H), 8.81 (d, J = 6.0 Hz, 1H), 8.54 (s, 1H), 8.43 (d, J = 6.0 Hz, 1H), 7.82 (s, 1H), 7.59 (d, J = 7.2 Hz, 2H), 7.42 (t, J = 7.8 Hz, 2H), 7.32 (s, 1H), 7.27 (t, J = 7.5 Hz, 1H), 2.82 (s, 3H).

1–[3–(4–fluorophenyl)–1*H*–pyrazolo[4,3–*c*]pyridin–6–yl]–3–[(1*R*)–1–phenylethyl]urea (**28**). *Step 1*. To a vial were added **3** (R^1 = 4–fluorophenyl) (73 mg, 0.15 mmol), (*R*)–1–(1–phenylethyl)urea (37 mg, 0.23 mmol), Cs_2CO_3 (120 mg, 0.367 mmol), BrettPhos precatalyst (11.7 mg, 0.015 mmol), and DMA (1.1 mL). The mixture was evacuated and purged with nitrogen six times and heated to 100 °C for 55 min. The mixture was diluted with EtOAc, washed with water and brine, dried over sodium sulfate, concentrated, and purified by flash chromatography to afford (*R*)–1–(3–(4–fluorophenyl)–1–trityl–1*H*–pyrazolo[4,3–*c*]pyridin–6–yl)–3–(1–phenylethyl)urea (85 mg, 0.14 mmol, 92% yield) as a yellow solid. LRMS (ESI) calcd for ($C_{40}H_{32}FN_5O$) $[M + H]^+$ 618, found 618. ^{1}H NMR (600 MHz, DMSO–d_6) δ 9.06 (s, 1H), 8.97 (s, 1H), 7.22–7.96 (m, 25H), 6.80 (s, 1H), 4.79 (m, 1H), 1.35 (d, J = 7.2 Hz, 3H).

Step 2. To a stirred solution of (*R*)–1–(3–(4–fluorophenyl)–1–trityl–1*H*–pyrazolo[4,3–*c*]pyridin–6–yl)–3–(1–phenylethyl)urea (61 mg, 0.10 mmol) in DCM (0.5 mL) were added TFA (0.5 mL) and triethylsilane (0.05 mL, 0.3 mmol). The mixture was stirred at room temperature for 10 min, concentrated, and purified by preparative–HPLC to afford **28** trifluoroacetate (40 mg, 0.083 mmol, 83% yield) as a yellow solid. HRMS (ESI) calcd for ($C_{21}H_{19}FN_5O$) $[M + H]^+$ 376.1573, found 376.1582. ^{1}H NMR (600 MHz, DMSO–d_6) δ 13.24 (s, 1H), 9.12 (s, 1H), 9.06 (s, 1H), 8.04 (dd, J = 8.8, 5.5 Hz, 2H), 7.75 (s, 1H), 7.65 (s, 1H), 7.39–7.27 (m, 6H), 7.22–7.18 (m, 1H), 4.86 (m, 1H), 1.39 (d, J = 6.9 Hz, 3H).

1–(3–Cyclopropyl–1*H*–pyrazolo[4,3–*c*]pyridin–6–yl)–3–[(1*R*)–1–phenylethyl]urea (**25**). Prepared in analogy to that described for **28** in 70% yield. HRMS (ESI) calcd for ($C_{18}H_{20}N_5O$) $[M + H]^+$ 322.1668, found 322.1674. ^{1}H NMR (600 MHz, DMSO–d_6) δ 12.57 (s, 1H), 8.98 (s, 1H), 8.74 (s, 1H),

7.88 (brs, 1H), 7.53 (s, 1H), 7.22–7.35 (m, 5H), 4.88 (m, 1H), 2.28 (m, 1H), 1.41 (d, *J* = 8.4 Hz, 3H), 0.95–1.02 (m, 4H).

1–[3–(1–Methyl–1*H*–pyrazol–4–yl)–1*H*–pyrazolo[4,3–*c*]pyridin–6–yl]–3–[(1*R*)–1–phenylethyl]urea (**27**). Prepared in analogy to that described for **28** in 50% yield. HRMS (ESI) calcd for ($C_{19}H_{20}N_7O$) $[M + H]^+$ 362.1729, found 362.1730. ^{1}H NMR (600 MHz, DMSO–d_6) δ 12.91 (s, 1H), 9.06 (s, 1H), 9.02 (s, 1H), 8.44 (s, 1H), 8.01 (s, 1H), 7.86 (brs, 1H), 7.61 (s, 1H), 7.24–7.36 (m, 5H), 4.90 (m, 1H), 3.92 (s, 3H), 1.42 (d, *J* = 8.4 Hz, 3H).

1–[3–(2,6–Dimethylpyridin–4–yl)–1*H*–pyrazolo[4,3–*c*]pyridin–6–yl]–3–[(1*R*)–1–phenylethyl]urea trifluoroacetate (**29**). Prepared in analogy to that described for **28** in 52% yield. HRMS (ESI) calcd for ($C_{22}H_{23}N_6O$) $[M + H]^+$ 387.1933, found 387.1946. ^{1}H NMR (600 MHz, CD_3OD) δ 9.33 (brs, 1H), 8.23 (s, 2H), 7.51 (brs, 1H), 7.18–7.35 (m, 5H), 3.28 (m, 1H), 2.79 (s, 6H), 1.51 (s, 3H).

1–[3–(2–Fluoropyridin–4–yl)–1*H*–pyrazolo[4,3–*c*]pyridin–6–yl]–3–[(1*R*)–1–phenylethyl]urea (**29**). Prepared in analogy to that described for **28** in 46% yield. HRMS (ESI) calcd for ($C_{20}H_{18}FN_6O$) $[M + H]^+$ 377.1526, found 377.1531. ^{1}H NMR (600 MHz, DMSO–d_6) δ 13.66 (s, 1H), 9.27 (s, 1H), 9.16 (s, 1H), 8.36 (d, *J* = 6.0 Hz, 1H), 8.01 (d, *J* = 6.0 Hz, 1H), 7.79 (s, 1H), 7.75 (s, 1H), 7.70 (brs, 1H), 7.23–7.36 (m, 5H), 4.90 (m, 1H), 1.42 (d, *J* = 8.4 Hz, 3H).

1–[3–(2–Methoxypyridin–4–yl)–1*H*–pyrazolo[4,3–*c*]pyridin–6–yl]–3–[(1*R*)–1–phenylethyl]urea trifluoroacetate (**31**). To a vial were added **8** (R^2 = (1*R*)–1–phenylethyl) (40 mg, 0.066 mmol), (2–methoxypyridin–4–yl)boronic acid (21 mg, 0.14 mmol), $PdCl_2$(dppf)–CH_2Cl_2 adduct (11 mg, 0.013 mmol), 1,4–dioxane (0.7 mL), and Na_2CO_3 (2 M, 0.1 mL, 0.2 mmol). The mixture was purged with nitrogen six times, heated to 80 °C for 3 h, and cooled to room temperature. The mixture was diluted with EtOAc, washed with water and brine, dried over sodium sulfate, and concentrated. The residue was dissolved in DCM (0.5 mL) and treated with TFA (0.5 mL) and triethylsilane (0.02 mL, 0.13 mmol). The mixture was stirred at room temperature for 16 h, concentrated, and purified by preparative–HPLC to afford **31** trifluoroacetate (14 mg, 0.028 mmol, 42% yield). HRMS (ESI) calcd for ($C_{21}H_{21}N_6O_2$) [M

+ H]$^+$ 389.1726, found 389.1736. ^{1}H NMR (600 MHz, DMSO–d_6) δ 13.58 (s, 1H), 9.24 (s, 1H), 9.19 (s, 1H), 8.30 (d, J = 4.8 Hz, 1H), 7.75 (m, 2H), 7.63 (dd, J = 5.4, 1.2 Hz, 1H), 7.23–7.38 (m, 6H), 4.90 (m, 1H), 3.93 (s, 3H), 1.43 (d, J = 7.2 Hz, 3H).

1–[3–(6–Methylpyridazin–4–yl)–1*H*–pyrazolo[4,3–*c*]pyridin–6–yl]–3–[(1*R*)–1–phenylethyl]urea trifluoroacetate (**32**). Prepared in analogy to that described for **31** in 38% yield. HRMS (ESI) calcd for ($C_{20}H_{20}N_7O$) [M + H]$^+$ 374.1729, found 374.1729. ^{1}H NMR (600 MHz, DMSO–d_6) δ 13.79 (s, 1H), 9.71 (s, 1H), 9.36 (s, 1H), 9.19 (s, 1H), 8.26 (s, 1H), 7.81 (s, 1H), 7.69 (brs, 1H), 7.25–7.36 (m, 5H), 4.90 (m, 1H), 2.75 (s, 3H), 1.43 (d, J = 6.6 Hz, 3H).

hERK2 Assay. Activated ERK2 activity was determined in an IMAP–FP assay (Molecular Devices). Using this assay format, the potency (IC_{50}) of each compound was determined from a 10 point (1:3 serial dilution, 3 μM starting compound concentration) titration curve using the following outlined procedure. To each well of a black Corning 384–well plate (Corning Catalog #3575), 7.5 nL of compound (3333 fold dilution in final assay volume of 25 μL) was dispensed, followed by the addition of 15 μL of kinase buffer (tween containing kinase buffer, Molecular Devices) containing 0.0364 ng/mL (0.833 nM) of phosphorylated active hERK2 enzyme. Following a 15 minute compound and enzyme incubation, each reaction was initiated by the addition of 10 μL kinase buffer containing 2.45 μM ERK2 IMAP substrate peptides (2.25 μM–unlabeled IPTTPITTTYFFFK–COOH and 200 nM–labeled IPTTPITTTYFFFK–5FAM (5–carboxyfluorescein)–COOH), and 75 μM ATP. The final reaction in each well of 25 μL consists of 0.5 nM hERK2, 900 nM unlabeled peptide, 80 nM labeled–peptide, and 30 μM ATP. Phosphorylation reactions were allowed to proceed for 60 minutes and were immediately quenched by the addition of 60 μL IMAP detection beads (1:1000 dilutions) in IMAP binding buffer (Molecular Devices) with 24 mM NaCl. Plates were read on EnVision reader after 60 minutes binding equilibration using Fluorescence Polarization protocol (Perkin Elmer).

pRSK Assay. Phospho–RSK in a BRAF mutant melanoma cell A375SM was quantified using mesoscale electrochemiluminescent sandwich assay. The potency (IC_{50}) of each compound was determined from 11 points titration curve. Briefly, 10,000 cells were seeded into a 384 well plate and incubated with compounds for 4 hours. Following removal of culture medium, cells were lysed at 4 ^{o}C for 20 minutes in 30 µL buffer containing 150 mM NaCl/20 mM Tris–HCl/1 mM EGTA/1 mM EDTA/1% Triton X/10 mM NaF plus protease and phosphatase inhibitors. Twenty microliter of cell lysates were transferred to a BSA–coated streptavidin–mesoscale plate. Biotin labeled anti–RSK1 (Enzo Life Science) and SULFO–TAG labeled anti–pRSK (pThr359/Ser363) (Epitomics) antibodies were diluted in assay buffer (PBS/0.2% Tween 20/2% BSA), and 10 µL of the diluted antibodies were added to the cell lysate. Following overnight incubation at 4 ^{o}C, plates were washed 3 times with PBS/0.05%Tween 20 buffer before read on MSD Sector S 600 in 1X MSD Read Buffer P.

Proliferation Assay. A375SM and CHL–1 cells suspended in DMEM/10 mM HEPES/10% FBS/Hyclone SH30071.03 were added (40 µL/well) to 384 Perkin Elmer Cultur plates subsequent to compound addition. Plates were incubated at 37 ^{o}C, 5% CO_2 for 96 hours. After incubation plates were equilibrated at room temperature for 15 minutes, proliferation was determined by addition of Cell Titer–Glo (Promega G7573) using the reagent protocol. Plates were read with a Perkin Elmer Spectrometer equipped with a luminescence protocol. Compound potency (IC_{50}) was determined by analysis of 10 point, 3–fold compound titration curves.

Supporting Information

Experimental procedures and spectral data for **2**, **13**, **14**, **16**, **19**, **20**, **22**, **24**, **26**; kinome data for **11**, **20**, **21**, **24**, **25**, **27**–**30**; X–ray statistics for **11**; PDB coordinates for docking poses of **9** and **10**. This material is available free of charge via the Internet at http://pubs.acs.org.

Accession Codes

PDB accession code of the structure of **11** bound to rat ERK2 is 5KE0. Authors will release the atomic coordinates and experimental data upon article publication.

Author Information

Corresponding Author

*Phone: 617−992−2012. E−mail: jongwon_lim@merck.com.

Notes

The authors declare no competing financial interest.

Acknowledgment

We thank Manami Shizuka for preparation of compound **21** for the in vivo studies, Melissa Chenard for designing the in vivo studies, and Wilfredo Pinto for analytical spectra of key compounds.

Abbreviations Used

ATP, adenosine triphosphate; AUC, area under the curve; BrettPhos precatalyst, chloro[2−(dicyclohexylphosphino)−3,6−dimethoxy−2',4',6'−triisopropyl−1,1'−biphenyl][2−(2−aminoethyl)phenyl]palladium(II); CDI, 1,1′−carbonyldiimidazole; Cl_p, plasma clearance; dba, dibenzylideneacetone; DPPA, phosphoric acid diphenyl ester azide; dppf, 1,1'− bis(diphenylphosphanyl) ferrocene; ERK, extracellular signal−regulated kinase; hERG, human ether−a−go−go related gene; LE, lignad efficiency; LiHMDS, lithium bis(trimethylsilyl)amide; MAPK, mitogen−activated protein kinase; MW, molecular weight; PK, pharmacokinetic; SAR, structure−activity relationship; V_{dss}, volume of distribution at steady state

References

(1) Roberts, P. J.; Der, C. J. Targeting the RAF–MEK–ERK mitogen activated protein kinase cascade for the treatment of cancer. *Oncogene* **2007**, *26*, 3291–3310.

(2) Uehling, D. E.; Harris, P. A. Recent progress on MAP kinase pathway inhibitors. *Bioorg. Med. Chem. Lett.* **2015**, *25*, 4047–4056.

(3) Chapman, P. B.; Hauschild, A.; Robert, C.; Haanen, J. B.; Ascierto, P.; Larkin, J.; Dummer, R.; Garbe, C.; Testori, A.; Maio, M.; Hogg, D.; Lorigan, P.; Lebbe, C.; Jouary, T.; Schadendorf, D.; Ribas, A.; O'Day, S. J.; Sosman, J. A.; Kirkwood, J. M.; Eggermont, A. M.; Dreno, B.; Nolop, K.; Li, J.; Nelson, B.; Hou, J.; Lee, R. J.; Flaherty, K. T.; McArthur, G. A. Improved survival with vemurafenib in melanoma with BRAF V600E mutation. *N. Engl. J. Med.* **2011**, *364*, 2507–2516.

(4) Hauschild, A.; Grob, J. J.; Demidov, L. V.; Jouary, T.; Gutzmer, R.; Millward, M.; Rutkowski, P.; Blank, C. U.; Miller, W. H., Jr; Kaempgen, E.; Martín–Algarra, S.; Karaszewska, B.; Mauch, C.; Chiarion–Sileni, V.; Martin, A. M.; Swann, S.; Haney, P.; Mirakhur, B.; Guckert, M. E.; Goodman, V.; Chapman, P. B. Dabrafenib in BRAF–mutated metastatic melanoma: a multicentre, open–label, phase 3 randomised controlled trial. *Lancet* **2012**, *380*, 358–365.

(5) Flaherty, K. T.; Robert, C.; Hersey, P.; Nathan, P.; Garbe, C.; Milhem, M.; Demidov, L. V.; Hassel, J. C.; Rutkowki, P.; Mohr, P.; Dummer, R.; Trefzer, U.; Larkin, J. M. G.; Utikal, J.; Dreno, B.; Nyakas, M.; Middleton, M. R.; Becker, J. C.; Casey, M.; Sherman, L. J.; Wu, F. S.; Quellet, D.; Martin, A. M.; Patel, K.; Schadendorf, D. Improved survival with MEK inhibition in BRAF–mutated melanoma. *N. Engl. J. Med.* **2012**, *367*, 107–114.

(6) Pratilas, C. A.; Solit, D. B. Targeting the mitogen–activated protein kinase pathway: physiological feedback and drug response. *Clin. Cancer Res.* **2010**, *16*, 3329–3334.

(7) Alcalá, A. M.; Flaherty, K. T. BRAF inhibitors for the treatment of metastatic melanoma: clinical trials and mechanisms of resistance. *Clin. Cancer Res.* **2012**, *18*, 33–39.

(8) Little, A. S.; Smith, P. D.; Cook, S. J. Mechanisms of acquired resistance to ERK1/2 pathway inhibitors. *Oncogene* **2013**, *32*, 1207–1215.

(9) Hatzivassiliou, G.; Liu, B.; O'Brien, C.; Spoerke, J. M.; Hoeflich, K. P.; Haverty, P. M.; Soriano, R.; Forrest, W. F.; Heldens, S.; Chen, H.; Toy, K.; Ha, C.; Zhou, W.; Song, K.; Friedman, L. S.; Almer, L. C.; Hampton, G. M.; Moffat, J.; Belvin, M.; Lackner, W. R. ERK inhibition overcomes acquired resistance to MEK inhibitors. *Mol. Cancer Ther.* **2012**, *11*, 1143–1154.

(10) Morris, E. J.; Jha, S.; Restaino, C. R.; Dayananth, P.; Zhu, H.; Cooper, A.; Carr, D.; Deng, Y.; Jin, W.; Black, S.; Long, B.; Liu, J.; Dinunzio, E.; Windsor, W.; Zhang, R.; Zhao, S.; Angagaw, M. H.; Pinheiro, E. M.; Desai, J.; Xiao, L.; Shipps, G.; Hruza, A.; Wang, J.; Kelly, J.; Paliwal, S.; Gao, X.; Babu, B. S.; Zhu, L.; Daublain, P.; Zhang, L.; Lutterbach, B. A.; Pelletier, M. R.; Philippar, U.; Siliphaivanh, P.; Witter, D.; Kirschmeier, P.; Bishop, W. R.; Hicklin, D.; Gilliland, D. G.; Jayaraman, L.; Zawel, L.; Fawell, S.; Samatar, A. A. Discovery of a novel ERK inhibitor with activity in models of acquired resistance to BRAF and MEK inhibitors. *Cancer Discovery* **2013**, *3*, 742–750.

(11) Chaikuad, A.; Tacconi, E. M. C.; Zimmer, J.; Liang, Y.; Gray, N. S.; Tarsounas, M.; Knapp, S. A unique inhibitor binding site in ERK1/2 is associated with slow binding kinetics. *Nat. Chem. Biol.* **2014**, *10*, 853–860.

(12) Foda, Z. H.; Seeliger, M. A. Kinase inhibitors: an allosteric add–on. *Nat. Chem. Biol*. **2014**, *10*, 796–797.

(13) Nissan, M. H.; Rosen, N.; Solid, D. B. ERK pathway inhibitors: how low should we go? *Cancer Discovery* **2013**, *3*, 719–721.

(14) Wong, D. J. L.; Robert, L.; Atefi, M. S.; Lassen, A.; Avarappatt, G.; Cerniglia, M.; Avramis, E.; Tsoi, J.; Foulad, D.; Graeber, T. G.; Comin–Anduix, B.; Samatar, A.; Lo, R. S.; Ribas, A. Antitumor activity of the ERK inhibitor SCH772984 against BRAF mutant, NRAS mutant and wild–type melanoma. *Mol. Cancer* **2014**, *13,* 194.

(15) Kinoshita, T.; Warizaya, M.; Ohori, M.; Sato, K.; Neya, M.; Fujii, T. Crystal structure of human ERK2 complexed with a pyrazolo[3,4–*c*]pyridazine derivative. *Bioorg. Med. Chem. Lett.* **2006**, *16*, 55–58.

(16) Aronov, A. M.; Baker, C.; Bemis, G. W.; Cao, J.; Chen, G.; Ford, P. J.; Germann, U. A.; Green, J.; Hale, M. R.; Jacobs, M.; Janetka, J. W.; Maltais, F.; Martinez–Botella, G.; Namchuk, M. N.; Straub, J.; Tang, Q.; Xie, X. Flipped out: structure–guided design of selective pyrazolylpyrrole ERK inhibitors. *J. Med. Chem.* **2007**, *50,* 1280–1287.

(17) Aronov, A. M.; Tang, Q.; Martinez–Botella, G.; Bemis, G. W.; Cao, J.; Chen, G.; Ewing, N. P.; Ford, P. J.; Germann, U. A.; Green, J.; Hale, M. R.; Jacobs, M.; Janetka, J. W.; Maltais, F.; Markland, W.; Namchuk, M. N.; Nanthakumar, S.; Poondru, S.; Straub, J.; ter Haar, E.; Xie, X. Structure–guided design of potent and selective pyrimidylpyrrole inhibitors of extracellular signal–regulated kinase (ERK) using conformational control. *J. Med. Chem.* **2009**, *52*, 6362–6368.

(18) Gerlach, M.; Seipelt, I.; Blumenstein, L.; Mueller, G.; Günther, E.; Schuster, T.; Teifel, M. Pyridopyrazine derivatives and their use. WO 2012/136691, 2012.

(19) Blake, J. F.; Gaudino, J. J.; De Meese, J.; Mohr, P.; Chicarelli, M.; Tian, H.; Garrey, R.; Thomas, A.; Siedem, C. S.; Welch, M. B.; Kolakowski, G.; Kaus, R.; Burkard, M.; Martinson, M.; Chen, H.; Dean, B.; Dudley, D. A.; Gould, S. E.; Pacheco, P.; Shahidi–Latham, S.; Wang, W.; West, K.; Yin, J.; Moffat, J.; Schwarz, J. B. Discovery of 5,6,7,8–tetrahydropyrido[3,4–*d*]pyrimidine inhibitors of ERK2. *Bioorg. Med. Chem. Lett.* **2014**, *24*, 2635–2639.

(20) Deng, D.; Shipps, G. W., Jr.; Cooper, A.; English, J. M.; Annis, D. A.; Carr, D.; Nan, Y.; Wang, T.; Zhu, H. Y.; Cheng, C. C.; Dayananth, P.; Hruza, A. W.; Xiao, J.; Jin, W.; Kirschmeier, P.; Windsor, W. T.; Samater, A. A. Discovery of novel, dual mechanism ERK inhibitors by affinity selection screening of an inactive kinase. *J. Med. Chem.* **2014**, *57*, 8817–8826.

(21) Ren, L.; Grina, J.; Moreno, D.; Blake, J. F.; Gaudino, J. J.; Garrey, R.; Metcalf, A. T.; Burkard, M.; Martinson, M.; Rasor, K.; Chen, H.; Dean, B.; Gould, S. E.; Pacheco, P.; Shahidi–Latham, S.; Yin, J.; West, K.; Wang, W.; Moffat, J. G.; Schwarz, J. B. Discovery of highly potent, selective, and efficacious small molecule inhibitors of ERK1/2. *J. Med. Chem.* **2015**, *58*, 1976–1991.

(22) Zhu, H. Y.; Desai, J.; Deng, Y.; Cooper, A.; Wang, J.; Shipps, J.; Samatar, A.; Carr, D.; Windsor, W. Discovery of hydroxyaniline amides as selective extracellular regulated kinase (ERK) inhibitors. *Bioorg. Med. Chem. Lett.* **2015**, *25*, 1627−1629.

(23) Ward, R.A.; Colclough, N.; Challinor, M.; Debreczeni, J. E.; Eckersley, K.; Fairley, G.; Feron, L.; Flemington, V.; Graham, M. A.; Greenwood, R.; Hopcroft, P.; Howard, T. D. James, M.; Jones, C. D.; Jones, C. R.; Renshaw, J.; Roberts, K.; Snow, L.; Tonge, M.; Yeung, K. Structure-guided design of highly selective and potent covalent inhibitors of ERK1/2. *J. Med. Chem.* **2015**, *58*, 4790–4801.

(24) Bagdanoff, J. T.; Jain, R.; Han, W.; Poon, D.; Lee, P. S.; Bellamacina, C.; Lindvall, M. Ligand efficient tetrahydro−pyrazolopyridines as inhibitors of ERK2 kinase. *Bioorg. Med. Chem. Lett.* **2015**, *25*, 3626–3629.

(25) Bagdanoff, J. T.; Jain, R.; Han, W.; Zhu, S.; Madiera, A.–M.; Lee, P. S.; Ma, X.; Poon, D. Tetrahydropyrrolo−diazepenones as inhibitors of ERK2 kinase. *Bioorg. Med. Chem. Lett.* **2015**, *25*, 3788–3792.

(26) Li, L.; Liu, F.; Jin, N.; Tang, S.; Chen, Z.; Yang, X.; Ding, J.; Geng, M.; Jiang, L.; Huang, M.; Cao, J. Discovery and structure activity relationship study of novel indazole amide inhibitors for extracellular signal-regulated kinase1/2 (ERK1/2). *Bioorg. Med. Chem. Lett.* **2016**, *26*, 2600–2604.

(27) Hopkins, A. L.; Groom, C. R.; Alex, A. Ligand efficiency: a useful metric for lead selection *Drug Discovery Today* **2004**, *9*, 430−431.

(28) Miyaura, N.; Suzuki, A. Palladium−catalysed cross−coupling reactions of organoboron compounds. *Chem. Rev.* **1995**, *95*, 2457–2483.

(29) Huang, X.; Buchwald, S. L. New ammonia equivalents for the Pd−catalyzed amination of aryl halides. *Org. Lett.* **2001**, *3*, 3417–3419.

(30) Breitler, S.; Oldenhuis, N. J.; Fors, B. P.; Buchwald, S. L. Synthesis of unsymmetrical diarylureas via Pd−catalyzed C−N cross−coupling reactions *Org. Lett.* **2011**, *13*, 3262– 3265.

(31) Manning, G.; Whyte, D. B.; Martinez, R.; Hunter, T.; Sudarsanam, S. The protein kinase complement of the human genome *Science* **2002**, *298*, 1912–1934.

(32) Friesen, R.; W.; Ducharme, Y.; Ball, R. G.; Blouin, M.; Boulet, L.; Cote, B.; Frenette, R.; Girard, M.; Guay, D.; Huang, Z.; Jones, T. R.; Laliberte, F.; Lynch, J. J.; Mancini, J.; Martins, E.; Masson, P.; Muise, E.; Pon, D. J.; Siegel, P. K. S.; Styhler, A.; Tsou, N. N.; Turner, M. J.; Young, R. N.; Girard, Y. Optimization of a tertiary alcohol series of phosphodiesterase–4 (PDE4) inhibitors: structure−activity relationship related to PDE4 inhibition and human ether−a−go−go related gene potassium channel binding affinity. *J. Med. Chem.* **2003**, *46*, 2413−2426.

Table of Contents Graphic